Fluctuating load perceived by the downstream turbine in a farm

Myriam Slama, Grégory Pinon, Yasmine Ben Belkacem, Camille Choma Bex, Michael Togneri, Iestyn Evans

Fluctuating load perceived by the downstream turbine in a farm

M. Slama, G. Pinon, Y. Ben Belkacem, C. Choma Bex, M. Togneri, I. Evans

***Abstract*—This paper presents computations of a four tidal turbine array, with a row of three upstream devices and a downstream turbine. The studied configuration is based on the layout initially proposed in the framework of the NEPTHYD project. The simulations were carried out with a three-dimensional unsteady Lagrangian Vortex software. A synthetic eddy method is used to take into account the ambient turbulence encountered in tidal energetic sites. The loads perceived by the turbines are estimated with a lifting line approach, recently added in the software. To study the interaction between the upstream and downstream turbines, numerical velocity maps, wake lines, unsteady velocity variations obtained with numerical probes as well as fluctuations of power and thrust coefficients are presented.**

***Index Terms*—Numerical computations; synthetic eddy method; tidal energy converters; turbulence; vortex method.**

I. Introduction

THE Atlantic Area interreg project named MONITOR proposed to study, via a multi-model approach, tidal turbine blade reliability. Several work-packages were design to carry out this study, such as the laboratory testing one, the numerical one or even the at-sea testing one based on full scale tidal prototypes. This 3 years project will end in late Autumn 2021; it is now time to review and summarise the work performed so far. The objective of the current paper is to present one of the topic treated in the numerical work-package.

In that respect, a 4 tidal turbine array representative of a commercial farm is considered for the present work (see Fig. 1). This turbine array is the NEPTHYD project formerly awarded to Alstom/General Electric - Engie for their project to the French 2013 call for tender [1]. Unfortunately, this project was stopped a couple of years ago due to the fact that General Electric decided to stop all tidal energy development at the time. However, this project is very interesting because first, it represents a real array configuration representative of a pre-commercial farm and second because the fourth turbine is positioned downstream of the 3 others during flood. Therefore, wake generated induced turbulence can then be estimated and compared to recent ambient measurement experimentally observed in-situ owing to several French research projects such as THYMOTE [2], [3] or HYD2M, for instance.

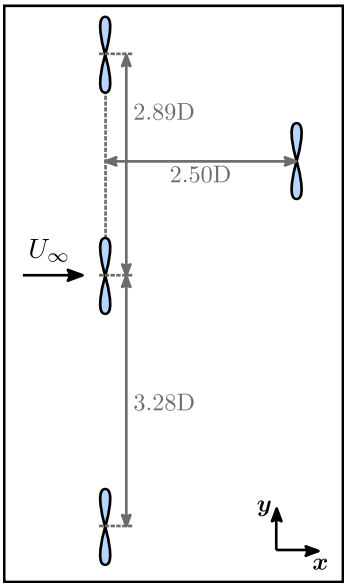

Fig. 1: Four tidal turbine array configuration based on the NEPTHYD project configuration and reproduced from information given in [1].

In a paper published recently [4], the numerical assessment of the ambient and wake generated turbulence level in this pre-commercial farm was studied. In case of a small tidal angular asymmetry, the wake of an upstream turbine can interact with the downstream one and therefore enhance the fluctuating load perceived by the downstream device. The Lagrangian software Dorothy was used with the latest features developed to take into account the ambient turbulence, such as the Synthetic Eddy Method proposed by Jarrin et al. [5] and recently adapted to the Lagrangian vortex framework [6]. For the present work, a lifting line method was added in the software to compute the torque and thrust for each turbine. A comparison between the fluctuating load perceived by an upstream turbine, only subjected to ambient turbulence, and the downstream turbine, subjected to a combined ambient+wake generated turbulence will be presented.

The ID number of this paper is 2227 of the conference track THM (Tidal Hydrodynamic Modelling). This work was supported in part by the European Regional Development Fund through the Interreg Atlantic Area Programme, via the MONITOR project. This work was also supported in part by the ERDF and the Normandy Regional Council via programs such as NEPTUNE, SEMARIN and DIADEMAR. CCB acknowledges the financial support of IFREMER for the funding of her Ph.D. grants. YBB acknowledges the financial support of Labex EMC3 programme Graduate School - Material and Energy Science. Some authors of this work are also co-financed by the European Regional Development Fund through the Interreg FCE (France Channel England), via the TIGER project. The present work was performed on computing resources provided by CRIANN (Normandy, France).

M. Slama, Y. Ben Belkacem and G. Pinon are with Normandie Univ, UNIHAVRE, UMR 6294 CNRS, LOMC 76600 Le Havre, France (e-mail: gregory.pinon@univ-lehavre.fr).

M. Togneri and I. Evans are with Energy & Environment Research Group, Swansea University, Bay Campus, Swansea SA1 8EN, UK.

II. Numerical method

A Lagrangian Vortex particle method is used in the Vortex Blob formulation. The Vortex method is an unsteady Lagrangian method, based on a discretisation of the flow into vorticity carrying particles [7], [8]. The governing equations for an unsteady and incompressible flow are the Navier-Stokes equations in their velocity/vorticity $(\boldsymbol{u}, \boldsymbol{\omega})$ formulation:

$$\nabla \cdot \boldsymbol{u} = 0, \tag{1}$$

$$\frac{D\boldsymbol{\omega}}{Dt} = (\boldsymbol{\omega} \cdot \nabla)\,\boldsymbol{u} + \nu \Delta \boldsymbol{\omega}, \tag{2}$$

where $\boldsymbol{u}$ is the velocity field, $\boldsymbol{\omega} = \nabla \wedge \boldsymbol{u}$ is the vorticity field and ν is the kinematic viscosity. A first adaptation of this numerical method to the tidal energy sector is presented in [9] using a panel integral method to represent the turbine blades.

For the present work, a lifting line will be preferred as a representation of the blades in order to have a better evaluation of the turbine torque and thrust force together with a more rapid calculation cost. The rotor blades are represented by several blade elements, for which the local relative velocity $\boldsymbol{V}_{\text{rel}}$ and angle of attack α are estimated at each time step (see Fig. 2). The loads are obtained using tabulated values for the lift and drag coefficients C_L and C_D (see [10] for more details).

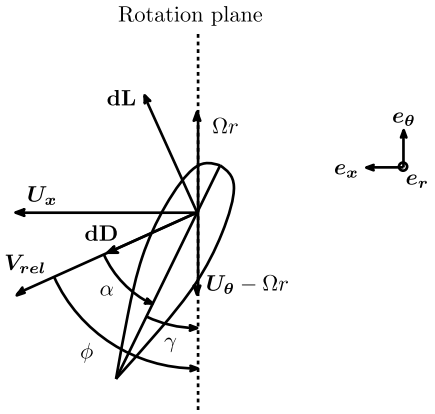

Fig. 2: Cross-sectional blade element.

Particles are emitted at the root and tip of each blade element. Their vorticity is estimated with a lifting line representation which is similar to the work of Murray et al. [11] for instance. The bound vortex attached to a blade element is related to the lift coefficient at any time t:

$$\Gamma_B(r,t) = \frac{1}{2} c V_{\text{rel}} C_L \tag{3}$$

where r is the spanwise dimension and c is the local chord. The trailing and spanwise vorticity shed in the wake, denoted by Γ_T and Γ_S respectively, are related to spanwise and temporal variations of Γ_B:

$$\Gamma_T\Big(r - \frac{\mathrm{d}r}{2}, t\Big) = \Gamma_B(r,t) - \Gamma_B(r - \mathrm{d}r, t) \tag{4}$$

$$\Gamma_S(r,t) = \Gamma_B(r, t - \mathrm{d}t) - \Gamma_B(r,t) \tag{5}$$

where $\mathrm{d}t$ is the time step and $\mathrm{d}r$ is the distance between two consecutive blade element centres.

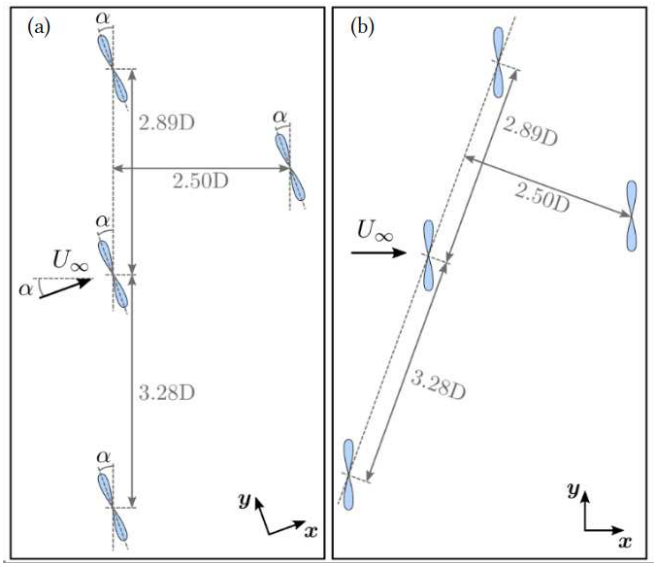

Fig. 3: Four tidal turbine array configuration based on the NEPTHYD project configuration and reproduced from information given in [1]. (a) Configuration with an incoming flow yawed with an angle α. (b) Similar representation but for which the flow is represented horizontally.

Finally, the ambient turbulence in the upstream flow is accounted for by modifying the upstream velocity which is rewritten via the use of a Reynolds decomposition:

$$\boldsymbol{u}_\infty(\boldsymbol{x},t) = \overline{\boldsymbol{u}_\infty}(\boldsymbol{x}) + \boldsymbol{u}'(\boldsymbol{x},t), \tag{6}$$

where $\overline{\boldsymbol{u}_\infty}$ is the mean velocity of the flow and $\boldsymbol{u}'$ its fluctuating part. This velocity fluctuating part $\boldsymbol{u}'$ is represented by a Synthetic Eddy Method (SEM). The representation of this fluctuating velocity $\boldsymbol{u}'$ is inspired from the work of Jarrin et al. [5] using a source and sink approximation of the turbulent structures. The fluctuating velocity $\boldsymbol{u}'$ could then be represented as:

$$\boldsymbol{u}'(\boldsymbol{x}) = \frac{1}{\sqrt{N}} \sum_{k=1}^{N} \boldsymbol{c^k} f_\lambda\Big(\frac{\boldsymbol{x} - \boldsymbol{x}^k}{\lambda}\Big), \tag{7}$$

where f_λ is a shape function and $\boldsymbol{c^k}$ is the intensity of a single turbulent structure k of centre point $\boldsymbol{x}^k$ and N the total number of turbulent structures. Much more numerical details are given in the recent work of Choma Bex et al. [6].

III. Numerical parameters

The schematic representation of Fig. 3 shows the turbines layout and spacing within the computation domain. An inclination of the incoming velocity vector is indicated in Fig. 3(a) with an angle α. Such a configuration with a yaw angle in the incident upstream velocity is tested in the present work as interactions will be highly enhanced between the middle upstream device and the downstream one as observed in Slama *et al.* [4]. Of course, as these turbines were supposed to be equipped with a yaw adaptation device, all the four turbines would reorient to align perfectly with the incoming flow. To facilitate the flow representation for

the following simulations presented in Section IV, the configuration of Fig. 3(b) is used. In this configuration, the turbines are yawed by an angle α = 10° so that the velocity vector always aligns with the x-axis. As the bathymetry cannot be taken into account in this study, the four turbines are set to the same vertical position.

The tidal turbine used for this study has a diameter D of 18 m. The blade characteristics and profiles correspond to the open-geometry turbine of IFREMER (French Research Institute for Exploitation of Sea). More details about IFREMER's turbine can be found in [4]. For the presented simulations, the rotor blades are modelled by a lifting line for which each blade is represented by 30 elements. Each blade element then has a length dr = 0.3 m discretizing the blade along the whole radius. The local value of the Reynolds number is taken into account for the polar curves used to evaluate the local lift and drag coefficients. The incoming upstream velocity was set to U_∞ = 3.2 m/s and the TSR (tip speed ratio) was set to 4.1, which corresponds to the optimal rotational speed of the devices. Further discretization and time parameters are considered, the inter-particle spacing is set to dh = 0.648 m with a smoothing parameter of $\delta = 1.5dh$, a time step of dt = 0.0479 s and the whole simulation time was set to t = 200 s.

In order to account for the ambient turbulence, an isotropic turbulence with an intensity of I_∞ = 10% is used, leading to 11339 turbulent structures to be considered following considerations mentioned in previous works [4], [6]. The size of each structure is λ = 4.5 m and its standard deviation is $\sigma(\lambda)$ = 75%. Moreover, a study space is defined where the turbulent structures will be placed, owing to the SEM contribution. The sizes of this space are $\mathscr{L}_x$ = 10D, $\mathscr{L}_y$ = 12D and $\mathscr{L}_z$ = 6D respectively along the flow axis, in width and vertically along the water depth.

IV. Results

Unless mentioned, all the following results are averaged over a time from t = 102 s to t = 182 s (representing 168 instantaneous velocity fields) in order to be fully converged. Moreover, for the sake of comparison, a computation was also performed without any ambient turbulence.

1) Velocity wake maps and wake lines:

Fig. 4 presents the computed velocity wake maps for the tested configuration. For the case considered without ambient turbulence I_∞ = 0%, an important interaction is observed between the middle upstream device and the downstream turbine. Besides, the wakes extension is very long and exceeds the 10D length presented in this figure. The account for ambient turbulence has modified the flow pattern when compared to the case without ambient turbulence. The wakes are shorter and other interaction phenomena are encountered mainly between the upper and middle upstream turbines wake and the downstream turbine. The results obtained for several configurations in [4] show that the value of the ambient turbulence intensity really has an important influence on the wake shape. This is further confirmed with these lifting lines computations and very similar observations can be drawn.

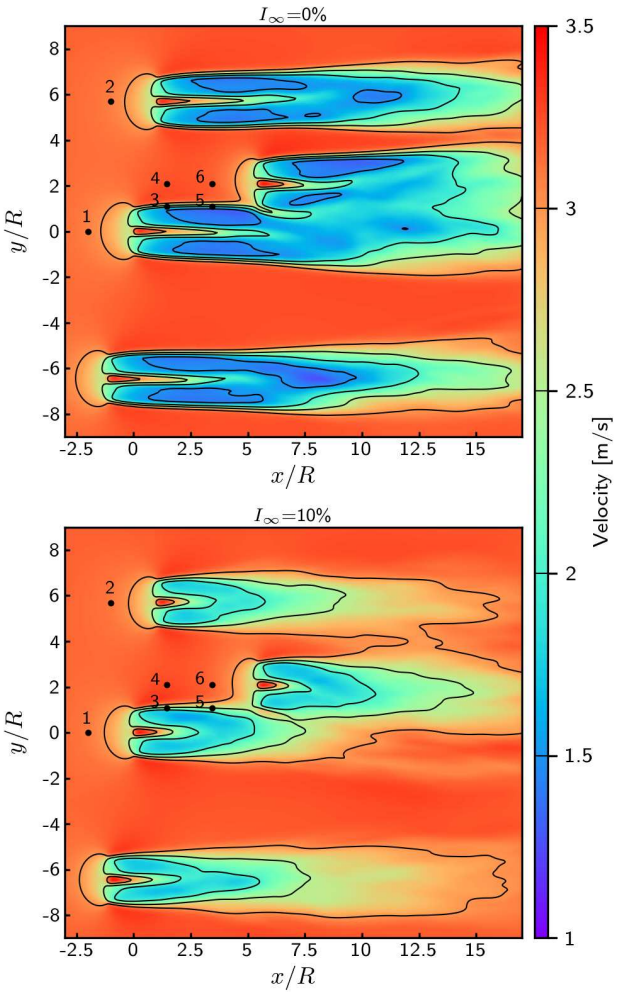

Fig. 4: Time-averaged velocity wake maps, I_∞=0% and I_∞=10%.

Fig. 5 depicts the corresponding wake lines of Fig. 4. They are taken from the turbines centre of rotation and are aligned with the turbines axis. Those lines represent the axial induction in front of each device. For these configurations, two of the upstream wake lines are similar and the third upstream wake line (purple dashed-dotted line) is a little bit modified, possibly due to the interaction mechanism with the downstream wakes. A small acceleration is also observed on the dotted lines upstream of the downstream turbine, mainly due to the Venturi effect imposed by the upper and middle upstream turbines. Similarly, a small acceleration is observed for the middle turbine line (dashed-dotted line) after the wake recorvery for the configuration with ambient turbulence I_∞ = 10%, most probably due to the bypass phenomenon too.

In addition, an important velocity deficit is observed in the case considered without ambient turbulence I_∞ = 0%. Finally, the upstream flow conditions are quickly recovered in the case with ambient turbulence, that is to say that the account of ambient turbulence significantly improves the results. As one can see,

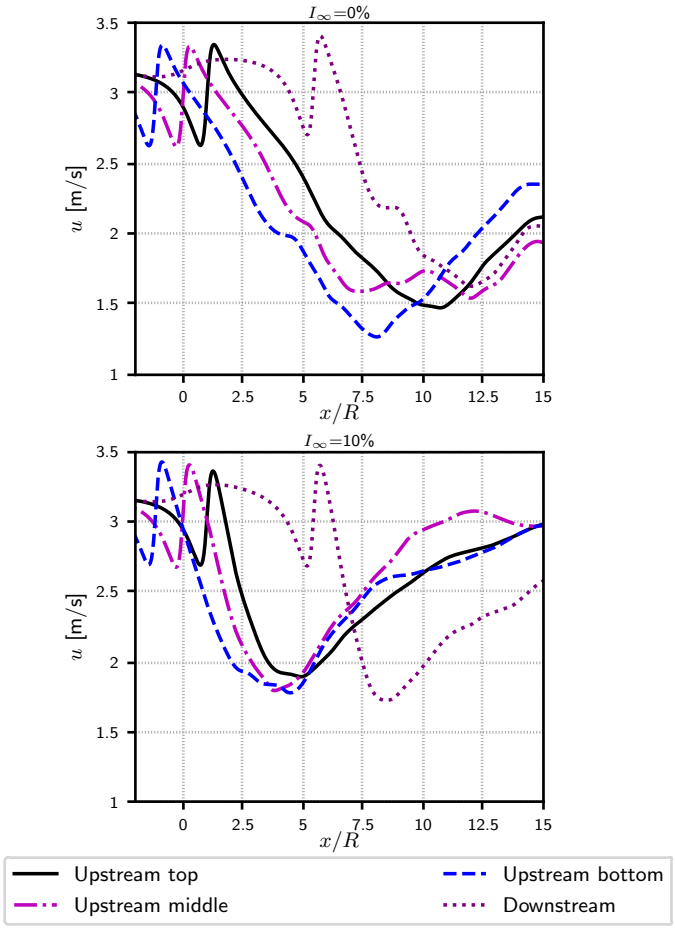

Fig. 5: Time-averaged wake lines, I_∞=0% and I_∞=10%.

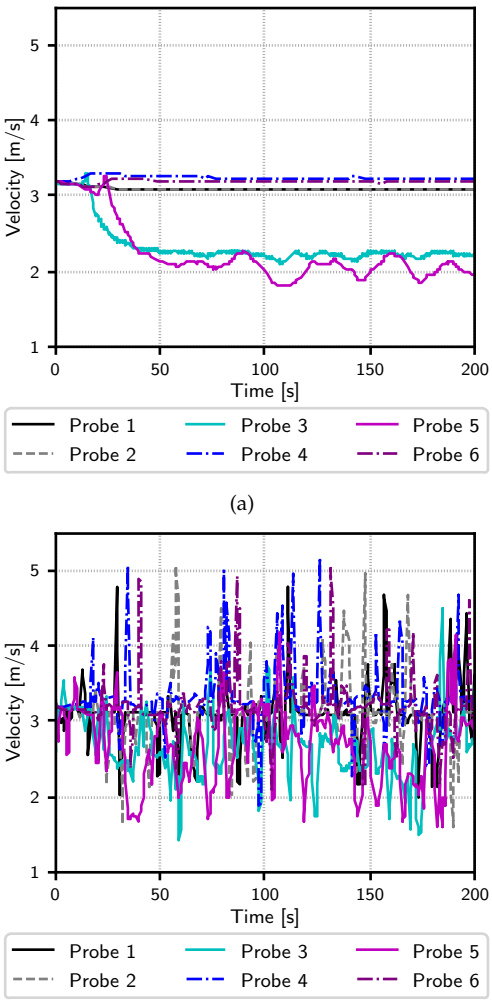

Fig. 6: Instantaneous velocity records measured at the different probe locations for: (a) I_∞=0% and (b) I_∞=10%.

some interesting physical phenomena are already present is these computations.

2) Velocity fluctuation based on the velocity probes:

Similarly to Slama *et al.* [4] and to better quantify the previous discussed phenomena, numerical probes were defined in the computation domain. These probes are represented by the points denoted from 1 to 6 in each plot of Fig. 4. Probes 1 and 2 are positioned one diameter upstream of the upper and middle upstream turbines respectively. These probes are included in order to give a reference value, as a matter to show the incoming flow disrupted only by ambient turbulence. Probes 4 and 6 are centred one and two diameters upstream of the downstream turbine respectively, whereas probes 3 and 5 are located in front of the blade tip of the downstream turbine, still one and two diameters upstream respectively. The velocity recorded by each probe for both cases are indicated in Fig. 6.

For the case with I_∞=0%, probes 1 and 2 show the unmodified incoming flow at the given incoming velocity of U_∞ = 3.2 m/s only slightly modified by the turbine axial induction. This can be further confirmed from the corresponding mean values presented in Table I with a velocity slightly lower than 3.1 m/s and a corresponding $\sigma(u)$ of 0.024 m/s each. These values can be identified as unmodified or *reference* values. Probes 4 and 6 present the velocity records in

TABLE I: Time-average $\overline{u}$ and the standard deviation $\sigma(u)$ of the velocity recorded by the probes at I_∞=0% (left) and I_∞=10% (right).

Probes	$I_\infty = 0\%$		$I_\infty = 10\%$	
	$\overline{u}$ [m/s]	$\sigma(u)$ [m/s]	$\overline{u}$ [m/s]	$\sigma(u)$ [m/s]
1	3.084	0.024	3.094	0.373
2	3.091	0.024	3.107	0.415
3	2.339	0.277	2.665	0.404
4	3.246	0.019	3.324	0.368
5	2.236	0.390	2.668	0.499
6	3.186	0.018	3.196	0.336

the by-pass depicting a combination of both physical effects: slightly accelerated flow in the by-pass and a velocity reduction owing to the downstream turbine axial induction, this last phenomenon being more and more important for probe 6 that is closer to the turbine. This is also evidenced by the corresponding data in Table I, also showing a very low velocity fluctuation for this I_∞=0%-case. On the contrary, for probes 3 and 5, increased values of the standard deviation of the velocity ($\sigma(u)$) are recorded, the higher value the closer to the turbine. This means that, locally for the tip of the downstream blade, high velocity fluctuations characterised by $\sigma(u)$ = 0.277 m/s and 0.390 m/s are

recorded, levels quasi equivalent to I_∞=10% ambient turbulence (see right hand-side of Table I for probes 1 and 2). This is mainly explained by the fact that these two probes are in the mixing layer of the middle upstream turbine wake, and the velocity fluctuation increases as the wake develops. Conversely, the corresponding averaged velocity values ($\overline{u}$) are decreasing as the wake evolves, with values such as 2.339 m/s and 2.236 m/s respectively.

For the I_∞=10% ambient turbulence case, many oscillations are observed on Fig. 6(b), potentially due to the passing of the turbulent structures. It is hardly impossible to observe tendencies from these time series, maybe except the slightly smaller values for probes 3 and 5. Therefore, the physical interpretations can only be done from either the time-average $\overline{u}$ and the standard deviation $\sigma(u)$ of the velocity and presented on the right hand-side of Table I. From the presented values for $\overline{u}$, very similar interpretations than for their I_∞=0% counterparts can be done. Very similar tendencies are observed, maybe except for probes 3 and 5, where the averaged velocity values are slightly higher owing to the fact that the wake is shorter, as depicted also in Fig. 4. This shorter wake is one of the interesting feature of the higher ambient turbulence. On the contrary, the standard deviations are all quite high, with values comprised between $0.370 \leq \sigma(u) \leq 0.415$ representing the ambient turbulence level, clearly identified for probes 1 and 2. Probes 4 and 6 show slightly lower values, possibly due to the by-pass effect and also identified for the I_∞=0%-configuration. The standard deviation of the velocity $\sigma(u)$ is in the ambient range for probe 3 but a reasonably higher value is observed for probe 5 with approximately $+25\%$ increase. This is most probably due to the combined effect of the ambient turbulence level and also the wake generated turbulence, this probe 5 being located in the mixing layer of the wake, as evidenced in Fig. 4(b). These observations are very similar to those already found in the previous study of Slama *et al.* [4] showing consistency in the results. However, the main advantage of using a lifting line resides in the possibility of assessing associated torque and thrust fluctuations, as is going to be presented in the following sub-section.

3) Turbine performance evaluation:

To evaluate the turbine performances, power and thrust coefficients are used and are respectively defined by:

$$C_P = \frac{Q \times \omega_x}{\frac{1}{2}\rho S U_\infty^3}, \tag{8}$$

$$C_T = \frac{F_x}{\frac{1}{2}\rho S U_\infty^2}, \tag{9}$$

where Q is the rotor torque, F_x is the rotor thrust, ω_x is the angular velocity in the x-direction and ρ is the fluid density. Fig. 7 shows the normalised power coefficients (C_P^*) obtained both for I_∞ = 0% and I_∞ = 10% and for the middle upstream turbine and the downstream one. Fig. 8 shows the exact equivalent but for the thrust coefficients (C_T^*). All the presented performance coefficients (C_P and C_T) were normalised (identified by *) by being divided by a reference value which is:

- the averaged C_P value over a time of 102s to 200s at I_∞=0% for the power coefficients.
- the corresponding averaged C_T value over the same duration and also for I_∞=0% for the thrust coefficients.

The obtained values for the normalised averaged power and thrust coefficients and their corresponding standard deviations are presented in Table II.

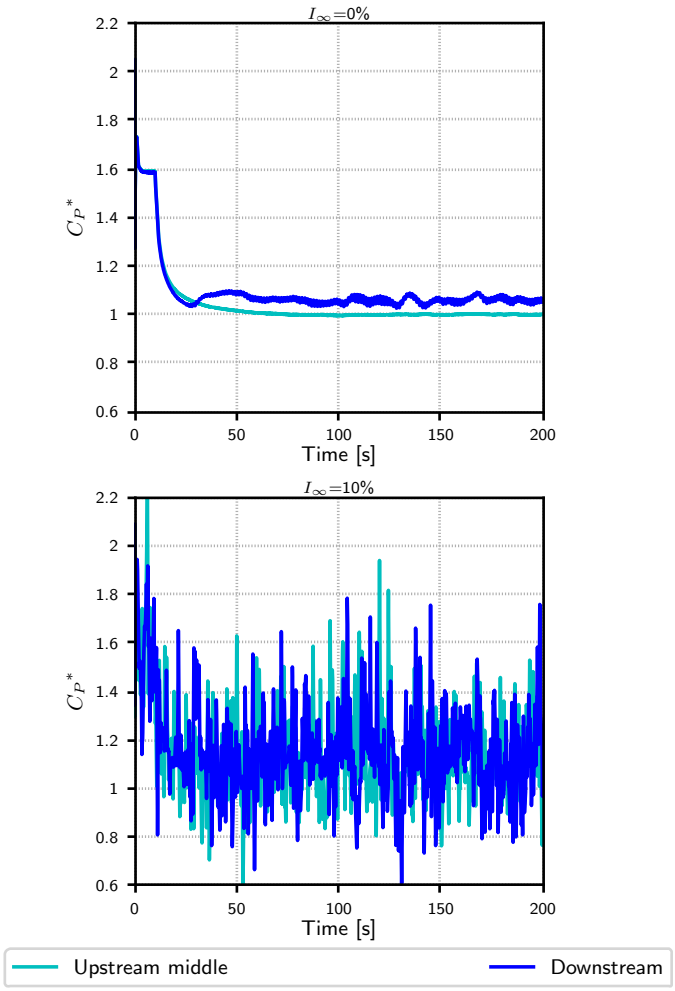

Fig. 7: Power coefficient, I_∞=0% and I_∞=10%

TABLE II: Normalised averaged power $\overline{C_P^*}$ and thrust $\overline{C_T^*}$ coefficients and their corresponding standard deviations $\sigma(\cdot)$ for the middle upstream turbine and the downstream one at I_∞ = 0 % and I_∞ = 10 %.

I_∞	I_∞ = 0%		I_∞ = 10%	
	upstr.	downstr.	upstr.	downstr.
$\overline{C_P^*}$	1.0000	1.0610	1.1298	1.1293
$\sigma(C_P^*)$	0.0013	0.0130	0.1507	0.1759
$\overline{C_T^*}$	1.0000	1.0306	1.0577	1.0562
$\sigma(C_T^*)$	0.0008	0.0080	0.0800	0.1025

For the case without ambient turbulence (I_∞=0%), both upstream values for C_P^* and C_T^* are very close to unity (Fig. 7(a) and Fig. 8(a)), also shown on the

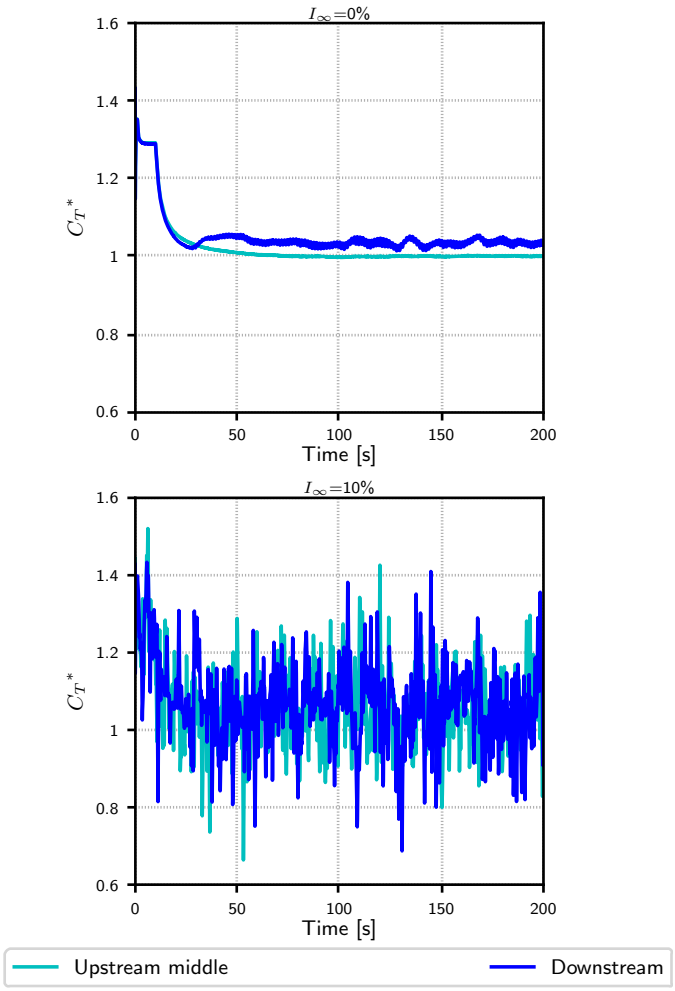

Fig. 8: Thrust coefficient, I_∞=0% and I_∞=10%

averaged corresponding values in Table II, with a unity value. This was expected and their corresponding standard deviation are also very low (see Table II). For the downstream turbine, an increase is obtained, both for the C_P^* (Fig. 7(a)) and C_T^* (Fig. 8(a)) most probably due to the flow acceleration in the by-pass. This increase results in an augmentation of approximately $+5\%$ in both $\overline{C_P^*}$ and $\overline{C_T^*}$ with respect to unity. However, a significant increase is already observable on the associated standard deviations $\sigma(C_P^*)$ and $\sigma(C_T^*)$ as one can see from Table II, although the absolute values keep fairly low ($\sigma(C_P^*)$=0.0130 m/s and $\sigma(C_T^*)$=0.0080 m/s). With these values, one can identify the associated load fluctuations only due to the wake generated turbulence, without any input from ambient turbulence.

On the contrary, from both Figs. 7(b) and 8(b) for an ambient turbulence of I_∞=10%, the instantaneous values of C_P^* and C_T^* show very high fluctuating levels. These increased levels of both $\sigma(C_P^*)$ and $\sigma(C_T^*)$ are both quite noticeable in Table II, for both upstream and downstream turbine. However, for this precise configuration with $\alpha = 10°$, the combined effect of wake generated turbulence is quasi hidden with the ambient turbulence fluctuating levels. Only a very small increase is observed from both downstream $\sigma(C_P^*)$ and $\sigma(C_T^*)$ quantities in comparison with their upstream values. For this geometrical configuration with a yaw angle of $\alpha = 10°$, only the tip part of the downstream turbine is impacted by the wake flow. Cases with $\alpha = 15°$ and $\alpha = 20°$ were tested in the study of Slama *et al.* [4] showing more and more intense interaction as the angle also increases. These four computations, corresponding to both I_∞=0%- or I_∞=10%-configurations for both higher angles, were not computed for the writing of this paper due to a lack of time. Hopefully, these results will be presented during the conference. A similar analysis could therefore be performed as presented in Togneri et al. [12] but taking into account the combined wake generated turbulence on top of the ambient turbulence level.

V. Conclusions and Prospects

The current communication aims at presenting computations of four tidal turbines in an array. The chosen array configuration is the one submitted by the consortium led by Alstom/General Electric - Engie for their project to the French 2013 call for tender [1] before General Electric stopped its tidal activities. It is therefore really representative of a real pre-commercial farm.

In these Lagrangian Vortex computations, the recently adapted Jarrin's formulation of the Synthetic Eddy Method is used as an ambient turbulence model. The ambient turbulence intensity used here is in the range of those presented in the literature from experimental campaigns performed in the Alderney Race, close to the location where the farm was supposed to be built. Depending on the upstream velocity yaw angle and ambient turbulence characteristics of the upstream tidal current, small to enhanced interaction can be presented. These interaction mechanisms can be identified either by the numerical velocity maps, wake lines or even numerical probes recording the unsteady velocity. For the downstream turbine, the perceived velocity can be highly modified by the wake interactions. With the very recent implementation of the lifting line, turbine performance evaluation, both in terms of power and trust coefficient, can also be assessed numerically. In the present paper, an extensive comparison was made for two ambient turbulence level (I_∞=0% and 10%) with a yaw angle of $\alpha = 10°$. Very interesting observations were already made, both in terms of averaged quantities or for their standard deviations. With such a numerical tool, assessment of combined ambient turbulence and wake generated turbulence influence on a downstream rotor can be studied. During the conference, more configurations with other yaw angles and/or possible different ambient turbulence levels will be presented in order to have a more comprehensive assessment of such interactions in a tidal farm.

References

[1] Autorit Environnementale, "Projet nepthyd," Conseil Général de l'environement et du développement durable : http://www.cgedd.developpement-durable.gouv.fr/IMG/pdf/160406_-_Hydroliennes_Raz_Blanchard_-_Nepthyd_50_-_delibere_cle05849f.pdf, Tech. Rep., last access

2021, March the 9th. [Online]. Available: http://www.cgedd.developpement-durable.gouv.fr/IMG/pdf/160406_-_Hydroliennes_Raz_Blanchard_-_Nepthyd_50_-_delibere_cle05849f.pdf

[2] M. Thibaut, J.-F. Filipot, C. Maisondieu, G. Damblans, R. Duarte, E. Droniou, N. Chaplain, and S. Guillou, "A comprehensive assessment of turbulence at a tidal-stream energy site influenced by wind-generated ocean waves," *Energy*, vol. 191, p. 116550, 2020. [Online]. Available: http://www.sciencedirect.com/science/article/pii/S0360544219322455

[3] A. Sentchev, M. Thiébaut, and S. Guillou, *Turbulence characterization at tidal-stream energy site in Alderney Race*, CRC press ed., 2020.

[4] M. Slama, C. Choma Bex, G. Pinon, M. Togneri, and I. Evans, "Lagrangian vortex computations of a four tidal turbine array: an example based on the NEPTHYD layout in the alderney race," *Energies*, vol. 14, no. 13, 2021. [Online]. Available: https://www.mdpi.com/1996-1073/14/13/3826

[5] N. Jarrin, S. Benhamadouche, D. Laurence, and R. Prosser, "A synthetic-eddy-method for generating inflow conditions for large-eddy simulations," *International Journal of Heat and Fluid Flow*, vol. 27, pp. 585–593, 2006.

[6] C. Choma Bex, C. Carlier, A. Fur, G. Pinon, G. Germain, and lie Rivoalen, "A stochastic method to account for the ambient turbulence in lagrangian vortex computations," *Applied Mathematical Modelling*, vol. 88, pp. 38 – 54, 2020. [Online]. Available: http://www.sciencedirect.com/science/article/pii/S0307904X20302614

[7] C. Rehbach, "Calcul numérique d'écoulements tridimensionnels instationnaires avec nappes tourbillonaires," *La Recherche Aérospatiale*, vol. 5, pp. 289–298, 1977.

[8] R. Lewis, *Vortex element methods for fluid dynamic analysis of engineering systems*. Cambridge University Press, 1991.

[9] G. Pinon, P. Mycek, G. Germain, and E. Rivoalen, "Numerical simulation of the wake of marine current turbines with a particle method," *Renewable Energy*, vol. 46, no. 0, pp. 111 – 126, 2012. [Online]. Available: http://www.sciencedirect.com/science/article/pii/S0960148112002418

[10] J. N. Sørensen and W. Z. Shen, "Numerical modeling of wind turbine wakes," *J. Fluids Eng*, vol. 124, no. 2, pp. 393–399, May 2002. [Online]. Available: https://doi.org/10.1115/1.1471361

[11] J. Murray and M. Barone, *The Development of CACTUS, a Wind and Marine Turbine Performance Simulation Code*. [Online]. Available: https://arc.aiaa.org/doi/abs/10.2514/6.2011-147

[12] M. Togneri, G. Pinon, C. Carlier, C. Choma Bex, and I. Masters, "Comparison of synthetic turbulence approaches for blade element momentum theory prediction of tidal turbine performance and loads," *Renewable Energy*, vol. 145, pp. 408 – 418, 2020. [Online]. Available: http://www.sciencedirect.com/science/article/pii/S0960148119307839